

# Time-dependent close-coupling calculations of the triple-differential cross section for electron-impact ionization of hydrogen

J. Colgan, M. S. Pindzola, and F. J. Robicheaux

*Department of Physics, Auburn University, Auburn, Alabama 36849*

D. C. Griffin

*Department of Physics, Rollins College, Winter Park, Florida 32789*

M. Baertschy

*JILA, Boulder, Colorado 80309*

(Received 30 November 2001; published 4 April 2002)

The formulation of the time-dependent close-coupling method is extended to allow the calculation of electron-impact triple-differential cross sections for atoms. The fully quantal method is applied to the electron-impact ionization of hydrogen at an incident energy of 54.4 eV for various scattering geometries. The time-dependent close-coupling results are found to be in very good agreement with those obtained by a time-independent exterior complex-scaling method. On the other hand, even though the incident energy is relatively large, significant differences are found between the two nonperturbative cross-section results and those obtained using perturbative distorted-wave methods. Large differences are found for those geometries that require an accurate knowledge of the correlation between two outgoing continuum electrons in the presence of a Coulomb nuclear field.

DOI: 10.1103/PhysRevA.65.042721

PACS number(s): 34.80.Dp

## I. INTRODUCTION

The electron-impact ionization of an atom yields two outgoing continuum electrons moving in the long-range Coulomb field of the remaining atomic ion; an example of a quantal three-body problem. The degree of interaction between the two continuum electrons depends on their overall energy, how they share that energy, and their angles of emission. An excellent probe of the correlation between the two outgoing electrons is the experimental measurement of the triple-differential cross section [1]. Although many relative and a few absolute measurements for various atoms have been made over the last 30 years, the first absolute triple-differential cross-section measurements for hydrogen near threshold were only recently reported [2].

A theoretical description of the electron-impact ionization of hydrogen begins with standard first-order perturbation theory [3,4]. The initial state is an incoming distorted-wave times the ground state of hydrogen, while the final state is a properly antisymmetrized product of outgoing distorted waves. As formulated, the standard first-order theory does not include any long-range correlation between the outgoing electrons; therefore, as will be shown in this paper, it has only a limited range of validity in the determination of triple-differential cross sections.

Many theoretical efforts have been made to extend the standard first-order perturbation theory for the electron-impact ionization of atoms [5]. These include the use of polarization potentials, final-state correlation factors, fractionally charged screening potentials, and the development of a variety of three-body continuum asymptotic wave functions. On the other hand, fully numerical nonperturbative methods [6–10] have been developed in the last decade, which yield total integral-electron-ionization cross sections for hydrogen,

which are all within the error bars of experimental measurements [11]. Two of the nonperturbative methods, the converged-close coupling [12] and the exterior complex scaling [13], have recently been applied to the calculation of absolute triple-differential cross sections for hydrogen near threshold.

In this paper, we extend the formulation of the time-dependent close-coupling method to enable the calculation of absolute triple-differential cross sections for the electron-impact ionization of hydrogen. Besides hydrogen, the time-dependent method has been used to calculate total-integral and single-differential cross sections for helium [14] and lithium [15], as well as total-integral cross sections for atomic ions in the helium [16], lithium [17,18], and sodium [19] isoelectronic sequences. In Sec. II, we present our formulation of the time-dependent close-coupling method for triple-differential, single-differential, and total-integral cross sections for the electron-impact ionization of hydrogen. We also include a short review of the time-independent perturbative distorted-wave and nonperturbative exterior complex-scaling methods. We then carry out triple-differential ionization calculations for hydrogen at an incident energy of 54.4 eV and present a variety of perturbative and nonperturbative results in Sec. III. In Sec. IV, we provide a full discussion and summary. Unless indicated otherwise, we use atomic units throughout this paper.

## II. THEORY

### A. Time-dependent close-coupling method

The time-dependent Schrödinger equation for the full six-dimensional dynamics of electron-hydrogen scattering is given by

$$i \frac{\partial \Psi(\vec{r}_1, \vec{r}_2, t)}{\partial t} = H(\vec{r}_1, \vec{r}_2) \Psi(\vec{r}_1, \vec{r}_2, t), \quad (1)$$

where the time-independent Hamiltonian is given by

$$H(\vec{r}_1, \vec{r}_2) = -\frac{1}{2} \nabla_1^2 - \frac{1}{2} \nabla_2^2 - \frac{1}{r_1} - \frac{1}{r_2} + \frac{1}{|\vec{r}_1 - \vec{r}_2|}. \quad (2)$$

The total wave function may be expanded in coupled spherical harmonics. From the projection onto the time-dependent Schrödinger equation, we obtain the following set of time-dependent close-coupled partial-differential equations for each  $LS$  symmetry:

$$\begin{aligned} i \frac{\partial P_{l_1 l_2}^{LS}(r_1, r_2, t)}{\partial t} &= T_{l_1 l_2}(r_1, r_2) P_{l_1 l_2}^{LS}(r_1, r_2, t) \\ &+ \sum_{l'_1, l'_2} U_{l_1 l_2, l'_1 l'_2}^L(r_1, r_2) P_{l'_1 l'_2}^{LS}(r_1, r_2, t), \end{aligned} \quad (3)$$

where  $T_{l_1 l_2}(r_1, r_2)$  contains kinetic energy, centrifugal barrier, and nuclear operators, while  $U_{l_1 l_2, l'_1 l'_2}^L(r_1, r_2)$  contains the electron two-body interaction that couples the various  $(l_1 l_2)$  scattering channels. This time-dependent close-coupling method is similar to an Euler angle time-dependent method developed by Bottcher [20] and is a wave packet solution to the same set of close-coupled partial-differential equations used in the time-independent electron-atom scattering method of Wang and Callaway [21,22].

The radial wave functions at time  $t=0$  are constructed as a simple product of the hydrogen ground state and an incoming radial wave packet

$$P_{l_1 l_2}^{LS}(r_1, r_2, t=0) = \delta_{l_1, 0} \delta_{l_2, L} P_{1s}(r_1) G_{kl_2}(r_2) (i)^{l_2} e^{-ikr_2}. \quad (4)$$

One propagates the radial wave functions for each  $LS$  symmetry according to the time-dependent close-coupled equations. At a time  $t=T$  following the collision, in which only outgoing waves are present in each channel, the momentum wave function for each  $LS$  symmetry is given by

$$\begin{aligned} P_{l_1 l_2}^{LS}(k_1, k_2) &= \int \int P_{k_1 l_1}(r_1) P_{k_2 l_2}(r_2) \\ &\times \bar{P}_{l_1 l_2}^{LS}(r_1, r_2, t=T) dr_1 dr_2, \end{aligned} \quad (5)$$

where

$$\bar{P}_{l_1 l_2}^{LS}(r_1, r_2, t) = \sqrt{\frac{1}{2}} [P_{l_1 l_2}^{LS}(r_1, r_2, t) + (-1)^S P_{l_1 l_2}^{LS}(r_2, r_1, t)], \quad (6)$$

and  $P_{kl}(r)$  are single-particle continuum orbitals that are normalized to one times a sine function. The triple-differential cross section for  $1s$  ionization is given by

$$\begin{aligned} &\frac{d^3 \sigma}{d\alpha d\Omega_1 d\Omega_2} \\ &= \frac{\pi}{4k^2} \sum_S (2S+1) \frac{2}{\pi} \int dk_1 \frac{2}{\pi} \int dk_2 \\ &\times \delta\left(\alpha - \tan^{-1}\left(\frac{k_2}{k_1}\right)\right) \left| \sum_L (i)^L \sqrt{2L+1} \right. \\ &\times \sum_{l_1, l_2} (-i)^{l_1+l_2} \exp[+i(\delta_{l_1} + \delta_{l_2})] \\ &\times P_{l_1 l_2}^{LS}(k_1, k_2) \sum_{m_1, m_2} C_{m_1 m_2 0}^{l_1 l_2 L} Y_{l_1 m_1}(\hat{k}_1) Y_{l_2 m_2}(\hat{k}_2) \left. \right|^2, \end{aligned} \quad (7)$$

where  $\alpha$  is the angle in the hyperspherical  $(k_1, k_2)$  plane,  $Y_{lm}(\vec{k})$  is a spherical harmonic, and  $C_{m_1 m_2 m_3}^{l_1 l_2 l_3}$  is a Clebsch-Gordan coefficient. The  $\delta(\alpha - \tan^{-1}(k_2/k_1))$  arises from conservation of energy in the hyperspherical plane. The single-differential cross section for  $1s$  ionization is given by

$$\begin{aligned} \frac{d\sigma}{d\alpha} &= \frac{\pi}{4k^2} \sum_{L,S} (2L+1)(2S+1) \frac{2}{\pi} \int dk_1 \frac{2}{\pi} \int dk_2 \\ &\times \delta\left(\alpha - \tan^{-1}\left(\frac{k_2}{k_1}\right)\right) \sum_{l_1, l_2} |P_{l_1 l_2}^{LS}(k_1, k_2)|^2. \end{aligned} \quad (8)$$

Finally, the total  $1s$  ionization cross section is given by

$$\sigma = \int_0^{\pi/2} \frac{d\sigma}{d\alpha} d\alpha = \int_0^E \frac{d\sigma}{dE_1} dE_1, \quad (9)$$

where the ejected energy  $E_1 = k_1^2/2$ , the total energy  $E = \epsilon_{1s} + k^2/2 = k_1^2/2 + k_2^2/2$ , and  $\epsilon_{1s}$  is the ground-state energy of hydrogen.

## B. Time-independent distorted-wave method

The time-independent radial Schrödinger equation for an incident distorted wave on the ground state of hydrogen is given by

$$\left[ T_l(r) + V_H(r) + V_X(r) - \frac{k^2}{2} \right] P_{kl}(r) = 0, \quad (10)$$

where  $T_l(r)$  contains kinetic energy, centrifugal barrier, and nuclear operators;  $V_H(r)$  is the direct Hartree potential;  $V_X(r)$  is a semiclassical exchange potential, and the radial distorted wave  $P_{kl}(r)$  is normalized to one times a sine function. Following standard first-order perturbation theory [3,4], we make two different choices for the distorted waves of the ejected and scattered electrons. In the first distorted-wave method (DW1) the scattered distorted wave is also a solution of Eq. (10), while the ejected distorted wave is a solution of

$$\left[ T_l(r) - \frac{k_1^2}{2} \right] P_{kl}(r) = 0. \quad (11)$$

The DW1 method has proved to be especially accurate for high angular momentum scattering. In the second distorted-wave method (DW2), both the ejected and scattered distorted-waves are solutions of Eq. (11). The DW2 method is generally more accurate for low angular momentum scattering. There are, of course, several other choices for the potentials used in the first-order theory.

In the first-order perturbation theory the triple-differential cross section for  $1s$  ionization is given by

$$\frac{d^3\sigma}{d\epsilon d\Omega_1 d\Omega_2} = \frac{4}{k^3 k_1 k_2} \sum_S (2S+1) \left| \sum_L \mathbf{A}(LS\hat{k}_1\hat{k}_2) \right|^2, \quad (12)$$

where

$$\mathbf{A}(LS\hat{k}_1\hat{k}_2) = \sum_{l_1, l_2} \sum_{m_1, m_2} i^{l_1+l_2} \exp[+i(\delta_L + \delta_{l_1} + \delta_{l_2})] \times A(l_1 l_2 LS m_1 m_2) Y_{l_1 m_1}(\hat{k}_1) Y_{l_2 m_2}(\hat{k}_2), \quad (13)$$

$$A(l_1 l_2 LS m_1 m_2) = (-1)^L (2L+1) \begin{pmatrix} l_1 & l_2 & L \\ 0 & 0 & 0 \end{pmatrix} \times \begin{pmatrix} l_1 & l_2 & L \\ m_1 & m_2 & 0 \end{pmatrix} M(l_1 l_2 LS), \quad (14)$$

$$M(l_1 l_2 LS) = \sqrt{\frac{2l_2+1}{2l_1+1}} R^{l_1}(k_1 l_1, k_2 l_2, 1s, kL) + (-1)^S \sqrt{\frac{2l_1+1}{2l_2+1}} R^{l_2}(k_2 l_2, k_1 l_1, 1s, kL), \quad (15)$$

$$R^\lambda(k_1 l_1, k_2 l_2, 1s, kL)$$

$$= \int_0^\infty dr_1 \int_0^\infty dr_2 P_{k_1 l_1}(r_1) P_{k_2 l_2}(r_2) \frac{r_{<}^\lambda}{r_{>}^{\lambda+1}} P_{1s}(r_1) P_{kL}(r_2), \quad (16)$$

where  $r_{<} = \min(r_1, r_2)$ ,  $r_{>} = \max(r_1, r_2)$ , and the standard expressions for  $3j$  symbols are employed. The single-differential cross section for  $1s$  ionization is given by

$$\frac{d\sigma}{dE_1} = \frac{4}{k^3 k_1 k_2 L_S} \sum_S (2L+1)(2S+1) \times \sum_{l_1, l_2} \begin{pmatrix} l_1 & l_2 & L \\ 0 & 0 & 0 \end{pmatrix}^2 [M(l_1 l_2 LS)]^2. \quad (17)$$

Finally, the total  $1s$  ionization cross section is given by

$$\sigma = \int_0^E \frac{d\sigma}{dE_1} dE_1. \quad (18)$$

### C. Time-independent exterior complex-scaling method

The time-independent Schrödinger equation for the full six-dimensional dynamics of electron-hydrogen scattering is rearranged to solve the outgoing scattered wave function according to

$$[E - H(\vec{r}_1, \vec{r}_2)] \Psi_{sc}^+(\vec{r}_1, \vec{r}_2) = [H(\vec{r}_1, \vec{r}_2) - E] \Psi_k^0(\vec{r}_1, \vec{r}_2), \quad (19)$$

where

$$\Psi_k^0(\vec{r}_1, \vec{r}_2) = \frac{1}{\sqrt{2}} [\Phi_{1s}(\vec{r}_1) e^{i\vec{k}\cdot\vec{r}_2} + (-1)^S \Phi_{1s}(\vec{r}_2) e^{i\vec{k}\cdot\vec{r}_1}], \quad (20)$$

and  $\Phi_{1s}(\vec{r})$  is the ground-state wave function of hydrogen. Following an expansion of the outgoing scattered wave function in coupled spherical harmonics and a mapping of the radial coordinates according to the method of exterior complex-scaling, we obtain a set of coupled, two-dimensional, complex-differential equations for each  $LS$  symmetry [10].

The triple-differential cross section for  $1s$  ionization is given by

$$\frac{d^3\sigma}{d\epsilon d\Omega_1 d\Omega_2} = \frac{8\pi^2}{k^2} |\mathbf{F}(\vec{k}_1, \vec{k}_2)|^2, \quad (21)$$

where the complex amplitude  $\mathbf{F}(\vec{k}_1, \vec{k}_2)$  may be obtained in terms of six-dimensional integrals involving Coulomb distorted waves and the outgoing scattered wave function [10,23]. The single-differential cross section for  $1s$  ionization is given by

$$\frac{d\sigma}{dE_1} = \frac{8\pi^2}{k^2} \sum_{L,S} \sum_{l_1, l_2} |f_{l_1 l_2}^{LS}(k_1, k_2)|^2, \quad (22)$$

where  $f_{l_1 l_2}^{LS}(k_1, k_2)$  are momentum amplitudes in a partial-wave expansion of  $\mathbf{F}(\vec{k}_1, \vec{k}_2)$ . Again, the total  $1s$  ionization cross section is given by

$$\sigma = \int_0^E \frac{d\sigma}{dE_1} dE_1. \quad (23)$$

## III. RESULTS

### A. Total-ionization cross section

Before considering differential cross sections for hydrogen at 54.4 eV, it is instructive to examine the partial-wave total-integral cross section at this energy. In Table I, we show the partial-wave total-integral cross section calculated using the time-dependent close-coupling method, the exterior complex-scaling method, and the two distorted-wave methods (DW1 and DW2). The two nonperturbative methods are in excellent agreement for all partial-wave cross sections and for the total cross section. The first distorted-wave method agrees quite well with the time-dependent method for the high angular momentum partial cross sections. We note that

TABLE I. Partial-wave total-ionization cross sections for hydrogen at 54.4 eV. TDCC denotes time-dependent close-coupling calculations; ECS denotes exterior complex-scaling calculations; DW1 and DW2 denotes distorted-wave calculations as discussed in the text. The total cross sections for TDCC include partial waves calculated using TDCC from  $L=0-9$  topped up with DW1 calculations from  $L=10-20$ , and the total cross sections for ECS include partial waves from  $L=0-13$  topped up with an extrapolation in  $L$  beyond this. The total cross sections for DW1 and DW2 include all partial waves up to and including  $L=20$ . All cross sections are in megabarns. ( $1.0 \text{ Mb} = 1.0 \times 10^{-18} \text{ cm}^2$ ).

$L$	TDCC	ECS	DW1	DW2
0	2.38	2.30	3.65	2.69
1	5.06	4.91	6.58	6.68
2	8.64	8.53	12.03	11.31
3	10.12	10.05	12.82	14.26
4	9.41	9.38	11.17	14.29
5	7.60	7.57	8.75	12.29
6	5.72	5.63	6.44	9.63
0-6	48.93	48.36	61.44	71.15
7	4.16	4.01	4.55	7.16
8	2.97	2.80	3.22	5.11
9	2.11	1.93	2.21	3.64
0-9	58.17	57.11	71.42	87.06
Total	62.76	62.23	76.02	95.70

the total cross section calculated using the time-dependent method for values of the orbital angular momentum  $L$  from 0-9 and topped up with DW1 results for  $L=10-20$  gives a cross section of 62.76 Mb, and that the exterior complex-scaling method gives a value of 62.23 Mb, both in excellent agreement with the experimental value of Shah *et al.* of 62 Mb [24].

However, here we wish to focus on the rate of convergence of the total-integral cross section with respect to the number of partial waves included in the calculation. By  $L=6$  the cross section has reached almost 80% of its final value and, by  $L=9$  the cross section has reached over 90% of its final value. This is common to all four of the calculations presented in Table I.

**B. Single-differential cross sections**

We now turn our attention to calculations of the single-differential cross section at 54.4 eV. In Table II we present the partial-wave contributions to the single-differential cross section at equal-energy sharing between the electrons for the same methods used in Table I. In this case, we see that by  $L=6$  the cross section has reached close to 95% of its final value and that by  $L=9$  the cross section has reached over 99% of its total value, again, for all four methods described. This demonstrates that, for the case where the energy available to the outgoing electrons is equally shared, convergence with respect to  $L$  is rapid and by  $L=6$  has almost reached its final value.

For cases where the ejected energy is not equally shared between the electrons, convergence with respect to  $L$  is not

TABLE II. As in Table I, but showing partial-wave single-differential cross sections at equal-energy sharing. All cross sections are in Mb/eV. ( $1.0 \text{ Mb} = 1.0 \times 10^{-18} \text{ cm}^2$ ).

$L$	TDCC	ECS	DW1	DW2
0	0.04	0.04	0.05	0.05
1	0.08	0.08	0.10	0.10
2	0.15	0.15	0.16	0.21
3	0.14	0.14	0.14	0.22
4	0.10	0.10	0.09	0.17
5	0.05	0.07	0.05	0.11
6	0.04	0.04	0.03	0.06
0-6	0.60	0.61	0.62	0.92
7	0.02	0.02	0.02	0.03
8	0.01	0.01	0.01	0.02
9	0.01	0.01	0.01	0.01
0-9	0.64	0.65	0.66	0.98
Total	0.65	0.66	0.66	0.98

so fast. For example, it was found that when one of the electrons carries 5 eV (and so the other has 35.8 eV), convergence of the single-differential cross section with respect to  $L$  is less rapid and, in fact, shows the same pattern as seen in Table I, by  $L=9$  the cross section has reached approximately 90% of its final value. For more extreme unequal-energy-sharing conditions the convergence is correspondingly slower.

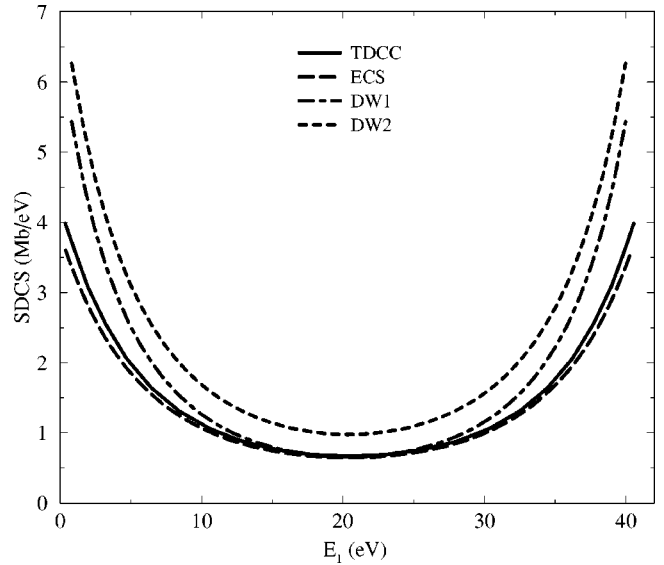


FIG. 1. Single-differential cross sections for hydrogen at 54.4 eV incident energy over a range of  $E_1$ , the energy of the first ejected electron. The time-dependent close-coupling (TDCC) calculations are given by the solid lines, the exterior complex scaling (ECS) calculations are given by the long-dashed line; the DW1 calculations are given by the dot-dashed line; and the DW2 calculations are given by the short-dashed line. The TDCC and ECS calculations include orbital angular momenta  $L$  from 0 to 9, and the distorted-wave calculations include values of  $L$  from 0 to 20. ( $1.0 \text{ Mb} = 1.0 \times 10^{-18} \text{ cm}^2$ .)

In Fig. 1 we present this single-differential cross section as calculated by all four methods over a range of the energy of the first ejected electron  $E_1$ . As expected, the characteristic “smile” shape of the single-differential cross section is reproduced. The time-dependent calculations (solid line) and the exterior complex-scaling calculations (long-dashed line) are clearly in excellent agreement over the full range of  $E_1$  as has also been previously demonstrated for several partial waves at a lower incident electron energy [25]. Both nonperturbative calculations include  $L$  from 0 through 9. Distorted-wave results are also presented for both the DW1 (dot-dashed line) and DW2 (short-dashed line) methods and are very similar in shape, although generally higher in magnitude than the nonperturbative results. However, we note that the cross section from the DW1 method is in surprisingly good agreement with the cross sections from the nonperturbative methods in the equal-energy-sharing region.

### C. Triple-differential cross sections: Convergence studies

There have already been many calculations exploring triple-differential cross sections over a wide range of excess electron energies and ejection angles. Here, we examine such calculations at an incident energy of 54.4 eV in an effort to check our new formulation of the time-dependent close-coupling method against the exterior complex-scaling method and to compare both nonperturbative methods with the perturbative distorted-wave method.

In all the calculations presented here we define  $\theta_1$  and  $\theta_2$ , the angles of the ejected and scattered electrons, as positive in the counterclockwise direction with respect to the incident electron-beam axis. This is specified clearly here since other groups have used different conventions in regard to this choice.

The time-dependent close-coupling equations for the two-electron radial wave functions were solved on a numerical lattice with uniform mesh spacing of 0.2 a.u. over a grid that extended to 50 a.u. The momentum wave functions were calculated using typically 300 continuum-state radial orbitals on a uniform momentum mesh with spacing  $\Delta k = 0.01$ . The time propagation of the radial wave functions was carried out until the collision probabilities were well converged. It was found that for particular combinations of electron angles and energies, where correlation effects would be expected to dominate the triple-differential cross section, it was necessary to time propagate the wave function over a much longer time and over a larger grid in order to achieve fully converged results. This was most evident in cases of equal-energy sharing between the electrons when the electrons were emitted along the same angle. Electron-electron correlation effects ensure that this cross section should go to zero in this region, but the convergence tends to be very slow. This demonstrates that calculation of the triple-differential cross section provides the most sensitive test of theory. However, for most other cases, where the angles or energies of the emitted electrons are not the same, convergence with respect to grid size and the propagation time was much more rapid.

Care must also be taken in testing convergence with respect to the number of angular momenta  $l_1 l_2$  pairs included in each partial wave  $L$ , as well as convergence with respect to the total number of  $L$  partial waves. It was found that, in general, many more  $l_1 l_2$  pairs were needed to converge the triple-differential cross section than to converge the total integral or single-differential cross section for each  $L$ . For example, even for a low  $L$  partial wave, such as  $^1P$ , up to 12  $l_1 l_2$  pairs were needed to converge the triple-differential cross section, whereas the total-integral and single-differential cross sections for  $^1P$  were well converged with only 6  $l_1 l_2$  pairs. Increasing the number of  $l_1 l_2$  pairs increases the size of the calculations accordingly. We comment here that the CPU time required for the time-dependent calculations to produce the wave functions in momentum space are of a similar magnitude to the exterior complex-scaling calculations of the complex amplitudes, and that both these are several orders of magnitude slower than the distorted-wave calculations. In the time-dependent calculations presented here we included a maximum of 22  $l_1 l_2$  pairs for the higher  $L$  partial waves. Therefore, these high  $L$  partial waves may not be completely converged, but their contribution to the triple-differential cross section is smaller than that of the lower partial waves.

### D. Triple-differential cross sections at fixed values of $\theta_2$

We now present comparison of the calculated triple-differential cross sections using all four methods previously described. Figs. 2–4 show the triple-differential cross section for values of the first ejected electron angle ( $\theta_1$ ) equal to  $30^\circ$ ,  $60^\circ$ , and  $90^\circ$ , respectively, over a range of  $\theta_2$  (the angle of the second ejected electron), for equal-energy-sharing conditions between the electrons. We compare results from (1) the time-dependent calculations [Figs. 2(a), 3(a), 4(a)]; (2) the exterior complex-scaling calculations [Figs. 2(b), 3(b), 4(b)]; (3) the distorted-wave DW1 calculations [Figs. 2(c), 3(c), 4(c)]; and (4) the distorted-wave DW2 calculations [Figs. 2(d), 3(d), 4(d)].

In parts (a) and (b) of Figs. 2–4 the long-dashed lines signify calculations including orbital angular momentum values  $L=0-6$  and the solid lines  $L=0-9$ . It is clear that for the calculations including only  $L=0-6$  the two nonperturbative methods give results that are in very good agreement. The  $L=0-9$  calculations, while reasonably close, are not in such good agreement. This is likely to be due to the insufficient number of  $l_1 l_2$  channels in the time-dependent calculations. For example, for  $L=7$  the time-dependent calculations included 22  $l_1 l_2$  channels, whereas the exterior complex-scaling calculations included 34  $l_1 l_2$  channels. For lower values of  $L$  the number of  $l_1 l_2$  channels used by both nonperturbative calculations were similar and we see the agreement between them is very good. This agreement also extends to the agreement between the two nonperturbative methods in the triple-differential cross sections for each individual  $L$  value. For  $L=7$  and beyond, we limited the number of  $l_1 l_2$  channels in the time-dependent calculations in an effort to determine the importance of the number of channels to the convergence of the triple-differential cross section. We see

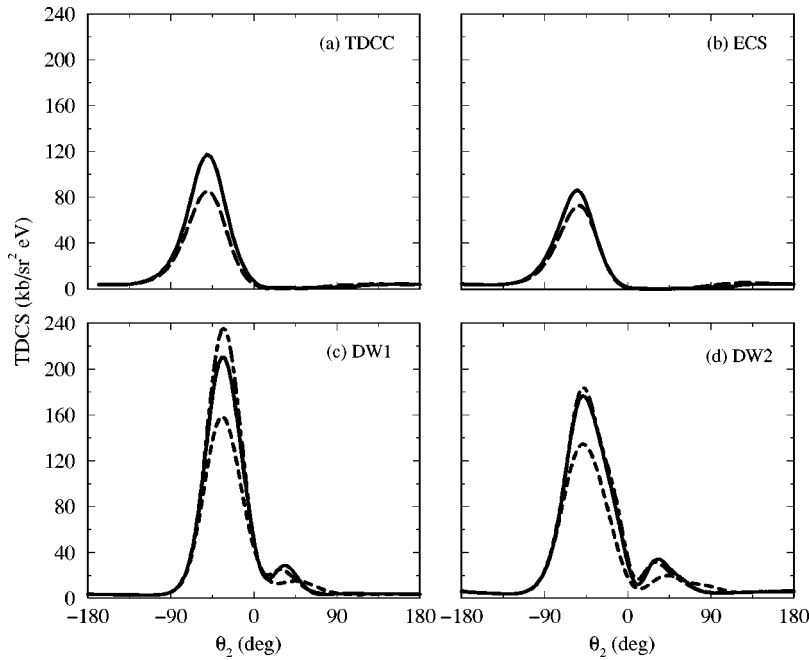


FIG. 2. Triple-differential cross section for hydrogen at 54.4 eV incident energy, for equal-energy sharing between the two electrons for  $\theta_1 = 30^\circ$  and over a range of  $\theta_2$ . Results are shown for the time-dependent close-coupling (TDCC), exterior complex-scaling (ECS), and the two distorted-wave (DW1 and DW2) methods. We present TDCC and ECS calculations that include orbital angular momentum values for  $L=0-6$  (long-dashed lines) and  $L=0-9$  (solid lines). The distorted-wave (DW1) and distorted-wave (DW2) calculations include orbital angular momentum contributions for  $L=0-6$  (short-dashed lines);  $L=0-9$  (dot-dashed lines); and  $L=0-20$  (solid lines). ( $1.0 \text{ kb} = 1.0 \times 10^{-21} \text{ cm}^2$ .)

that the poorer agreement for the  $L=0-9$  calculations demonstrates that the number of channels included is central to the convergence of the triple-differential cross section.

The distorted-wave results, parts (c) and (d) of Figs. 2–4 are for three total  $L$  values:  $L=0-6$  (short-dashed line),  $L=0-9$  (dot-dashed line), and  $L=0-20$  (solid line). For  $\theta_1 = 30^\circ$  (Fig. 2) the cross sections are noticeably higher than the nonperturbative cross sections, especially for the DW1 calculations. We also see that there is little difference between the distorted-wave results for  $L=0-9$  and  $L=0-20$ , indicating convergence with respect to  $L$ . This gives us confidence that our nonperturbative calculations in parts (a) and (b) of Figs. 2–4 are reasonably well converged with respect to  $L$ . This is also supported by the excellent convergence by

$L=9$  of the single-differential cross section at equal-energy sharing, as discussed previously. A similar trend in convergence is seen for  $\theta_1 = 60^\circ$ . In this case, the distorted-wave DW1 cross section is now lower than the nonperturbative cross sections whereas the DW2 cross section continues to be higher than the nonperturbative cross sections. Also, for  $\theta_1 = 90^\circ$ , the DW1 cross section is now considerably lower than those obtained from the nonperturbative methods and the cross section resulting from the DW2 method is of a similar height to those obtained from the nonperturbative methods.

The nonperturbative and distorted-wave results show the same broad shape in the cross section. However, the distorted-wave curves consistently have an extra peak in the

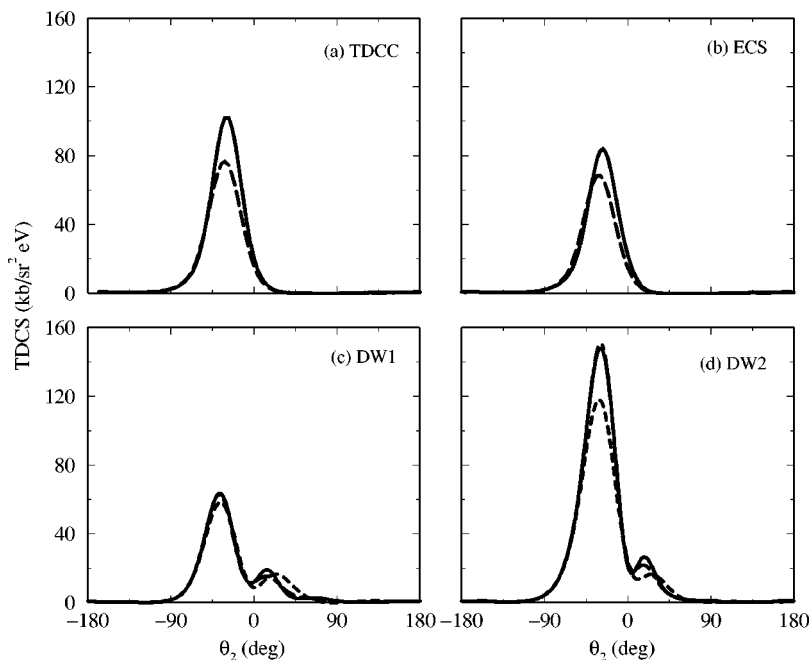


FIG. 3. Same as Fig. 2, for the case where  $\theta_1 = 60^\circ$ . ( $1.0 \text{ kb} = 1.0 \times 10^{-21} \text{ cm}^2$ .)

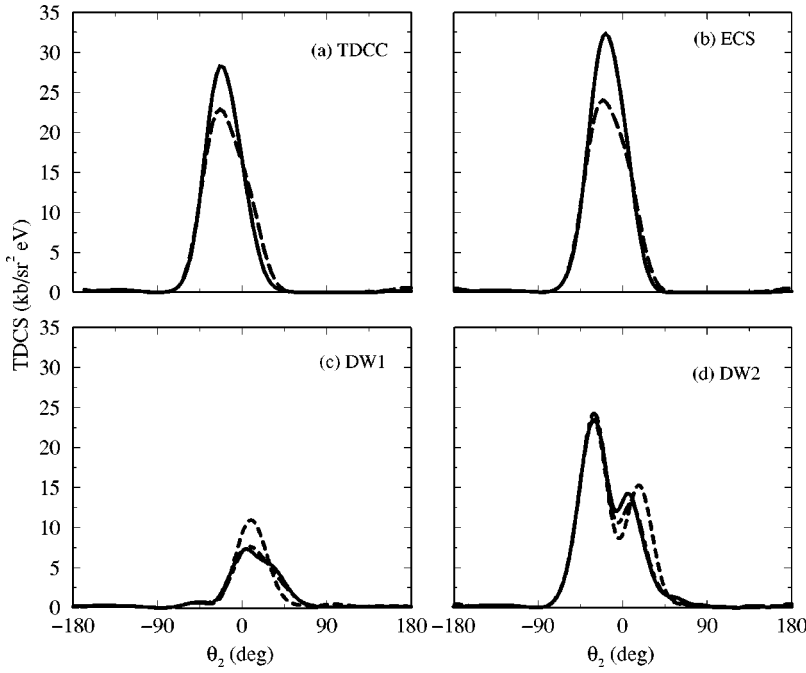


FIG. 4. Same as Fig. 2, for the case where  $\theta_1 = 90^\circ$ . ( $1.0 \text{ kb} = 1.0 \times 10^{-21} \text{ cm}^2$ .)

cross section around low positive values of  $\theta_2$ , which is clearly unphysical. This is due to the incomplete treatment of electron-electron correlation in the distorted-wave theory.

#### E. Triple-differential cross sections at fixed values of $\theta_{12}$

In Fig. 5, we present the triple-differential cross section for the case where the angle between the ejected electrons  $\theta_{12}$  (defined simply as  $\theta_{12} = \theta_1 - \theta_2$ ) equals  $180^\circ$ . In this particular case of back-to-back emission of the electrons, the electron-electron correlation should be minimal (since the electrons are always as far apart as possible) and we would expect the distorted-wave results to give reasonable cross

sections. This is indeed what is found. Here we again compare in [Fig. 5(a)] the time-dependent, [Fig. 5(b)] exterior complex-scaling, [Fig. 5(c)] distorted-wave DW1, and [Fig. 5(d)] distorted-wave DW2 results. In this case, the cross sections from all four methods have good agreement in shape. The nonperturbative methods and the DW2 method also agree reasonably well in magnitude, with the DW2 result being slightly higher. However, the peaks in the DW1 cross section are considerably lower by a factor of 2 than those calculated by the other methods and the “trough” is correspondingly more shallow. This is interesting because, for the single-differential cross section, it is the DW1 method that unexpectedly agrees better with the nonperturbative methods

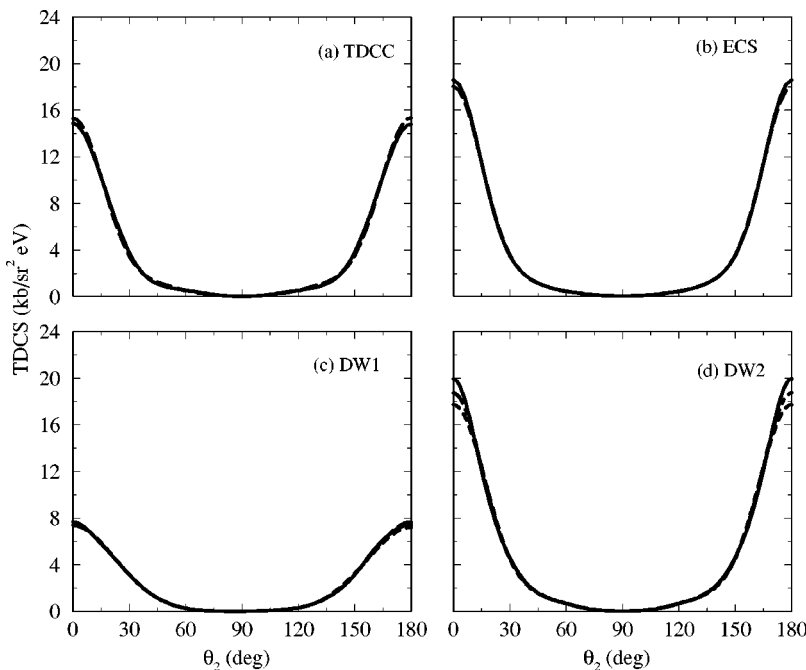


FIG. 5. Triple-differential cross section for hydrogen at 54.4 eV incident energy, for equal-energy sharing between the two electrons and for  $\theta_{12} = 180^\circ$ , where  $\theta_{12} = \theta_1 - \theta_2$ . As before we compare (a) the time-dependent (TDCC) method, (b) the exterior complex-scaling (ECS) method, (c) the DW1 method, and (d) the DW2 method. For (a) and (b) we show  $L=0-6$  (long-dashed lines) and  $L=0-9$  (solid lines), and in (c) and (d) we show  $L=0-6$  (short-dashed line),  $L=0-9$  (dot-dashed line), and  $L=0-20$  (solid line). ( $1.0 \text{ kb} = 1.0 \times 10^{-21} \text{ cm}^2$ .)

at equal-energy sharing. The DW2 results are in good agreement with the nonperturbative calculations. Again, for Figs. 5(a) and 5(b) we show results including  $L=0-6$  (long-dashed line) and  $L=0-9$  (solid line), and for Figs. 5(c) and 5(d) we show  $L=0-6$  (short-dashed line),  $L=0-9$  (dot-dashed line), and  $L=0-20$  (solid line). It is clear that the triple-differential cross section at this geometry is well converged even by  $L=6$  for all four methods. As expected for this back-to-back emission case, the cross section is at a maximum for  $\theta_2=0^\circ$  and  $180^\circ$ .

#### IV. SUMMARY

In this paper, we have extended the time-dependent close-coupling method to allow the calculation of electron-impact triple-differential cross sections for atoms. Results from our time-dependent method agree very well with nonperturbative time-independent calculations using the exterior complex-scaling method for calculations of total-integral, single-differential, and triple-differential cross sections for the electron-impact ionization of hydrogen at an incident electron energy of 54.4 eV. Cross sections resulting from perturbative distorted-wave calculations are generally larger than those obtained from the non-perturbative calculations and, for some cases, the distorted-wave methods yield anomalous shapes for triple-differential cross sections.

Here, as in previous time-dependent calculations, higher  $L$  contributions to total and single-differential cross sections were calculated using the distorted-wave method. This was possible since the extra contributions could be added to the time-dependent calculations incoherently. In the calculation of triple-differential cross sections, however, all contributions from each orbital angular momentum  $L$  must be added coherently. Also, we have seen that the distorted-wave method can give unphysical shapes in some regions of the triple-differential cross sections. This will be present for all angular momenta and so can introduce unphysical contributions if used to top up nonperturbative calculations. Of course, this is not the case for all geometries; for instance, for  $\theta_{12}=180^\circ$ , the distorted-wave methods yield cross sections with shapes similar to those obtained from the nonperturbative methods. In this case, however, we have seen that the triple-differential cross section converges quickly with respect to  $L$  and so top-up is not required.

Although we can now express some confidence in the use of the time-dependent method for the determination of triple-

differential cross sections, work remains in order to present triple-differential cross sections over the widest possible range of incident and ejected energies, as well as for different ejected geometries.

We have shown that, in the time-dependent method, large numbers of coupled channels are necessary to achieve convergence of the triple-differential cross sections for each  $L$ . This is further complicated by the fact that convergence with respect to the number of coupled channels varies widely for different ejected electron geometries, and is much slower when the energy sharing between ejected electrons is very asymmetric. However, we have seen that by studying convergence with respect to  $L$  for the total and single-differential cross sections, one can obtain some indication of the probable convergence of the triple-differential cross section for a particular value of the energy-sharing ratio. For lower incident energies, the convergence with respect to  $L$  is much more rapid and the nonperturbative methods are capable of producing converged triple-differential cross sections for a wide range of ejected electron geometries and energy sharings. Even at the relatively high incident energy of 54.4 eV we are confident that our results are reasonably well converged for equal-energy-sharing conditions and at the angles studied here. As the energy sharing becomes more asymmetric the maximum value of  $L$  needed for convergence increases and consequently convergence of the triple-differential cross section at highly unequal-energy sharing, for this incident electron energy, is not possible at this time using the current methods.

In future work, we intend to examine various approximations to the nonperturbative method to calculate the contribution from the higher angular momentum partial waves in a timely manner. Once accomplished, this will enable us to apply the time-dependent method to the calculation of electron-impact triple-differential cross sections for helium and the alkali metals. It is hoped that this work can stimulate further experimental measurements of absolute triple-differential cross sections.

#### ACKNOWLEDGMENTS

This work was supported in part by the U.S. Department of Energy, Office of Basic Energy Sciences and Office of Fusion Energy Sciences. Computational work was carried out at the National Energy Research Scientific Computing Center in Oakland, California.

- 
- [1] H. Ehrhardt, M. Schulz, T. Tekaas, and K. Willmann, *Phys. Rev. Lett.* **22**, 89 (1969).  
 [2] J. Roder, H. Ehrhardt, C. Pan, A. F. Starace, I. Bray, and D. V. Fursa, *Phys. Rev. D* **79**, 1666 (1997).  
 [3] S. M. Younger, in *Electron Impact Ionization*, edited by T. D. Märk and G. H. Dunn (Springer Press, Berlin, 1985), p. 1.  
 [4] I. E. McCarthy and Z. Xixiang, in *Computational Atomic Physics*, edited by K. Bartschat (Springer Press, Berlin, 1996), p. 87.  
 [5] S. P. Lucey, J. Rasch, and C. T. Whelan, *Proc. R. Soc. London, Ser. A* **455**, 349 (1999).  
 [6] I. Bray and A. T. Stelbovics, *Phys. Rev. Lett.* **70**, 746 (1993).  
 [7] D. Kato and S. Watanabe, *Phys. Rev. Lett.* **74**, 2443 (1995).  
 [8] K. Bartschat and I. Bray, *J. Phys. B* **29**, L577 (1996).  
 [9] M. S. Pindzola and F. Robicieux, *Phys. Rev. A* **54**, 2142 (1996).  
 [10] M. Baertschy, T. N. Rescigno, W. A. Isaacs, X. Li, and C. W. McCurdy, *Phys. Rev. A* **63**, 022712 (2001).  
 [11] M. B. Shah, D. S. Elliott, and H. B. Gilbody, *J. Phys. B* **20**, 3501 (1987).

- [12] I. Bray, *J. Phys. B* **33**, 581 (2000).
- [13] T. N. Rescigno, M. Baertschy, W. A. Isaacs, and C. W. McCurdy, *Science* **286**, 2474 (1999).
- [14] M. S. Pindzola and F. J. Robicheaux, *Phys. Rev. A* **61**, 052707 (2000).
- [15] J. Colgan, M. S. Pindzola, D. M. Mitnik, and D. C. Griffin, *Phys. Rev. A* **63**, 062709 (2001).
- [16] M. S. Pindzola, D. M. Mitnik, J. Colgan, and D. C. Griffin, *Phys. Rev. A* **61**, 052712 (2000).
- [17] M. S. Pindzola, F. J. Robicheaux, N. R. Badnell, and T. W. Gorczyca, *Phys. Rev. A* **56**, 1994 (1997).
- [18] D. M. Mitnik, M. S. Pindzola, D. C. Griffin, and N. R. Badnell, *J. Phys. B* **32**, L479 (1999).
- [19] N. R. Badnell, M. S. Pindzola, I. Bray, and D. C. Griffin, *J. Phys. B* **31**, 911 (1998).
- [20] C. Bottcher, *J. Phys. B* **15**, L463 (1982).
- [21] Y. D. Wang and J. Callaway, *Phys. Rev. A* **48**, 2058 (1993).
- [22] Y. D. Wang and J. Callaway, *Phys. Rev. A* **50**, 2327 (1994).
- [23] M. Baertschy, T. N. Rescigno, and C. W. McCurdy, *Phys. Rev. A* **64**, 022709 (2001).
- [24] M. B. Shah, D. S. Elliott, and H. B. Gilbody, *J. Phys. B* **20**, 3501 (1987).
- [25] M. Baertschy, T. N. Rescigno, and C. W. McCurdy, J. Colgan, and M. S. Pindzola, *Phys. Rev. A* **63**, 050701(R) (2001).